ISSN 0036-0244, Russian Journal of Physical Chemistry A, 2019, Vol. 93, No. 4, pp. 736–742. © Pleiades Publishing, Ltd., 2019.

PHYSICAL CHEMISTRY OF NANOCLUSTERS AND NANOMATERIALS

Synthesis and Enhanced Photocatalytic Activity of Visible-Light-Driven Co-Doped Bi_2MoO_6 Photocatalyst with Flower-Like Nanostructures[1]

Jie Wang[a], Yangang Sun[a,*], Zeming Wang[a], Chongchong Wu[a], and Pinhua Rao[a,]**

[a] *College of Chemistry and Chemical Engineering, Shanghai University of Engineering Science, Shanghai, 201620 China*

** e-mail: syg021@sues.edu.cn*

*** e-mail: raopinhua@hotmail.com*

Received April 12, 2018; revised April 12, 2018; accepted April 12, 2018

Abstract—Co-doped Bi_2MoO_6 photocatalyst has been synthesized by a simple and facile solvothermal method. It exhibits the flower-like microspheres composed of orthorhombic Bi_2MoO_6 nanoplates with the increase of the Co doping amount from 0 to 0.4%. Among these Co-doped samples, 0.1% Co–Bi_2MoO_6 sample shows the degradation efficiency of 99.7% for Rhodamine B under visible-light-irradiation within 120 min, which is higher than pure Bi_2MoO_6 and other Co-doping Bi_2MoO_6 flower-like microspheres. The calculated apparent reaction rate constant for the 0.1% Co–Bi_2MoO_6 of 0.0298 ± 0.0028 min^{-1} is 4.18 times of pure Bi_2MoO_6 photocatalyst (0.0071 ± 0.0010 min^{-1}). The flower-like microspheres of 0.1% Co–Bi_2MoO_6 with high efficient photocatalytic performance is a promising photocatalytic material.

Keywords: Bi_2MoO_6, codoping, photocatalyst, nanomaterials

DOI: 10.1134/S0036024419040307

1. INTRODUCTION

Semiconductor photocatalysis is a effective, green and potential method for the degradation of many toxic organic pollutants from aqueous systems because of its low cost, simplicity and high efficiency [1–3]. Industrial application of this technology is depended on developing efficient and stable visible-light-driven photocatalysts [4–6]. A significant progress of the photocatalysts has been made, and the photocatalysts have shown the great promise in degradation of organic pollutants from industrial wastewater by utilizing sunlight [7–10]. Many photocatalysts with a wide bandgap limit their availability to irradiation light [11–15]. Consequently, it is necessary to develop the visible light driven semiconductor photocatalysts for effective utilization of the solar spectrum.

Bismuth-base oxide semiconductors, such as Bi_2O_3, BiOX (X = Cl, Br, I), Bi_2WO_6, $BiVO_4$, and Bi_2MoO_6 [16, 17], have been demonstrated to show superior photocatalytic activities under visible-light irradiation because of Bi 6*s* and O 2*p* levels forming a preferable hybridized conduction band to exhibit strong oxidative ability for degradation of organic pollutants [18, 19]. Bi_2MoO_6 with flower-like microspheres consisted of nanosheets has been widely studied due to the excellent electrical property, high light absorption and abundant reactive sites [20]. However, photocatalytic performance of Bi_2MoO_6 is seriously limited by high recombination efficiency of photogenerated electron-hole pairs [21]. To enhance the photocatalytic performance, many materials [22] have been developed to improve the photocatalytic capability of Bi_2MoO_6, a large number of studies showed that Bi_2MoO_6 doped with different element can effectively improve the photocatalytic activity compared to pure nanostructures. For example, Cl-doped Bi_2MoO_6 as visible light driven photocatalyst was synthesized by hydrothermal method, and showed higher photocatalytic degradation of rhodamine B than pure Bi_2MoO_6 [23]. W-doped Bi_2MoO_6 nanoplates photocatalyst [24] with the increase of the W doping amount from 0 to 3% exhibit increased photodegradation efficiency for RhB under visible light irradiation. The property of Ce-doped Bi_2MoO_6 nanoplates demonstrated that the well-engineered crystal defects could boost electron dynamics by trapping effects and mediate the band structure by introducing new energy levels, leading to an enhanced photocatalytic activity [25].

Inspired by these previous reports, here we have synthesized flower-like Bi_2MoO_6 doped with Co by a solvothermal method. The photocatalytic activity of Co-doped Bi_2MoO_6 was investigated under visible

[1] The article is published in the original.

light irradiation, and they displayed high performance and stability for the photodecomposition of rhodamine B (RhB).

2. EXPERIMENTAL

2.1. Preparation of Pure-Bi_2MoO_6 and Co-Doped Bi_2MoO_6

All reagents were analytically pure and used without further purification. Co-doped Bi_2MoO_6 with different Co/Bi molar ratios (0.00, 0.05, 0.1, 0.2, 0.3, and 0.4%) were prepared by a one-step solvothermal method. In a typical solvothermal synthesis, firstly, 2 mmol of $Bi(NO_3)_3 \cdot 5H_2O$ (0.97 g) was dissolved in 20 mL of ethylene glycol and magnetically stirred for 30 min, then 1 mmol of $Na_2MoO_4 \cdot 2H_2O$ (0.242 g) was added to the above solution and stirred for 30 min at room temperature. Second, a certain amount of $Co(C_5H_7O_2)_3$ (0.0, 2.57, 5.14, 10.28, 15.42, and 20.56 mg for 0.0, 0.05, 0.1, 0.2, 0.3, and 0.4%, respectively) was dissolved in 20 mL of ethanol and stirred for 20 min. Third, ethanol solution with different amounts of $Co(C_5H_7O_2)_3$ was added to the mixtures of $Bi(NO_3)_3 \cdot 5H_2O$ and $Na_2MoO_4 \cdot 2H_2O$, and the mixed solution was stirred continuously for 2 h. Subsequently, the mixed solution was transferred into a 50 mL Teflon-lined stainless steel autoclave and heated in an oven at 160°C for 20 h. After the reaction, the autoclave was cooled down to room temperature in air, the sample was then collected by centrifugation and washed with ethanol and deionized water several times, and dried at 70°C for 12 h. Bi_2MoO_6 with different Co/Bi molar ratios were obtained, and named the sample pure-Bi_2MoO_6, 0.05% Co–Bi_2MoO_6, 0.1% Co–Bi_2MoO_6, 0.2% Co–Bi_2MoO_6, 0.3% Co–Bi_2MoO_6, and 0.4% Co–Bi_2MoO_6, respectively.

2.2. Characterizations

The structures and purity of the as-prepared products were characterized by X-ray diffraction (XRD, Rigaku D/max-2550 PC X-ray powder diffractometer). The morphology and size of the samples were observed using a field emission scanning electron microscope (SEM, S-4800) with an energy dispersive X-ray spectrometer (EDS). Transmission electron microscopy (TEM) and high-resolution TEM (HRTEM) images were acquired on a JEM-2100F high-resolution transmission electron microscope with the acceleration voltage of 200 kV. X-ray photoelectron spectroscopy (ESCALab MKII spectrometer with an excitation source of Mg-Ka radiation) analysis was used to determine the chemical binding states of the constituent elements. UV–Vis diffuse reflectance spectroscopy (DRS) was performed on UV3600 spectrophotometer. The mass of $Co(C_5H_7O_2)_3$ powder were weighed by electronic analytical balance (METTLER TOLEDO XS105DU, max weight = 41 g, d = 0.01 mg).

2.3. Photocatalytic Activity Experiments

Rhodamine B (RhB, the maximum absorption peak 554 nm) is a popular probe molecule in heterogeneous catalytic reactions because of being a typical dye resistant to biodegradation and direct photolysis. For the evaluation of catalytic activity, degradation experiments of the RhB dye were carried out under visible light at ambient temperature. The experimental procedures are as follows, 20 mg of the photocatalyst sample was added into RhB solution (50 mL, 5.0 mg L^{-1}) to form a suspension. Afterwards, the suspension was kept in the dark under magnetic stirring for 60 min to ensure an adsorption/desorption equilibrium. Then, the suspension under magnetic stirring was placed approximately 10 cm below a xenon lamp (500 W, Model PLS-SXE300) with a cut-off filter that only emits visible light ($\lambda > 400$ nm). At each sampling time (20 min), the irradiation was switched off and the suspension of about 3.5 mL was taken and centrifuged. The absorbance spectrum of RhB solution was analyzed using a UV-1901 spectrophotometer. After testing, the solution was returned and the irradiation was resumed.

3. RESULTS AND DISCUSSION

3.1. Structure and Morphology

The crystalline structure of the samples was determined by X-ray diffraction (XRD) measurements. Figure 1a shows the XRD patterns of the 0.0–0.4% Co-doped Bi_2MoO_6. In the XRD pattern of pure Bi_2MoO_6 sample, all diffraction peaks match well with the standard orthorhombic Bi_2MoO_6 structure (JCPDS no. 21-0102). No obvious peaks of other impurities were detected, indicating that high quality orthorhombic phase Bi_2MoO_6 sample was obtained via current synthetic method. In the XRD pattern of Co-doped Bi_2MoO_6 samples, no new peak is observed in the Co-doped Bi_2MoO_6 sample. The careful observation from the Fig. 1b indicates that the intensity of the diffraction peaks in all Co-doped Bi_2MoO_6 samples obviously decreases by comparing with pure Bi_2MoO_6 sample. Moreover, a minor shift of the (140) and (131) diffraction peaks of Co-doped Bi_2MoO_6 also takes place in comparing to pure Bi_2MoO_6 due to the different element Co doping, as shown in Fig. 1c. Therefore, the XRD analysis confirms that the Co was incorporated into the Bi_2MoO_6 lattices by a simple solvothermal method.

To further understand the function of Co ions doping, X-ray photoelectron spectroscopy (XPS) was performed to investigate the chemical states of doped Co ions and bismuth and molybdenum atoms in the dis-

torted crystal of 0.1% Co–Bi_2MoO_6, the survey scan of XPS spectra of 0.1% Co-doped Bi_2MoO_6 is shown in Fig. 2a. It was found that the binding energies peaks of Bi located at 158.9 and 164.2 eV. They are identified to Bi $4f_{7/2}$ and Bi $4f_{5/2}$, as shown in Fig. 2b. Figure 2c shows the binding energies at 232.2 and 235.4 eV of Mo in 0.1% Co–Bi_2MoO_6 which are assigned to Mo $3d_{5/2}$ and Mo $3d_{3/2}$ of Mo^{6+}. The O 1*s* region can be fitted into two peaks at 529.7 and 531.1 eV, which are attributed to binding energies of Bi–O and Mo–O bonding Fig. 2d [24]. The binding energies values of Co show two binding energies peaks at 805.3 and 781.3 eV in accordance with Co $2p_{1/2}$ and Co $2p_{3/2}$ in 0.1% Co–Bi_2MoO_6 Fig. 2e [26, 27], indicating the chemical state of Co^{3+} in Co-doped Bi_2MoO_6.

The morphology and size of Bi_2MoO_6 and 0.1% Co–Bi_2MoO_6 nanostructures were firstly observed by scanning electron microscopy (SEM). Figures 3a and 3b are the images of pure-Bi_2MoO_6, and the sample is composed of the small assemblies and the big flower-like microspheres. The small assemblies are consisted of several nanosheets, and these microspheres with diameters of ~2 μm are built from two dimensional (2D) nanosheets with the thickness of 20 nm. The 0.1% Co–Bi_2MoO_6 nanostructures present microspherical morphology with diameters ranging from 1 to 3.5 μm, as shown in Figs. 3c and 3d. With the Co content increasing, the Co doped Bi_2MoO_6 nanostructures display the flower-like shape similar to 0.1% Co–Bi_2MoO_6. The TEM image further verifies that the flower-like microsphere of 0.1% Co–Bi_2MoO_6 is consisted of 2D nanosheets with the nanoparticles on the surface (Fig. 3e). The high-resolution TEM image (Fig. 3f) clearly displays two types of lattice fringes. The crystal planes with lattice fringe spacing of 0.236 and 0.328 nm correspond to the (221) and (140) crystallographic plane of orthorhombic Bi_2MoO_6, respectively. Furthermore, the EDS pattern (Fig. 4) further confirms that 0.1% Co–Bi_2MoO_6 consists of Bi, O, Mo, and Co elements. Based on XRD, XPS, SEM, TEM, and EDS characterizations, one can confirm the well formation of the flower-like Co-doped Bi_2MoO_6 microsphere.

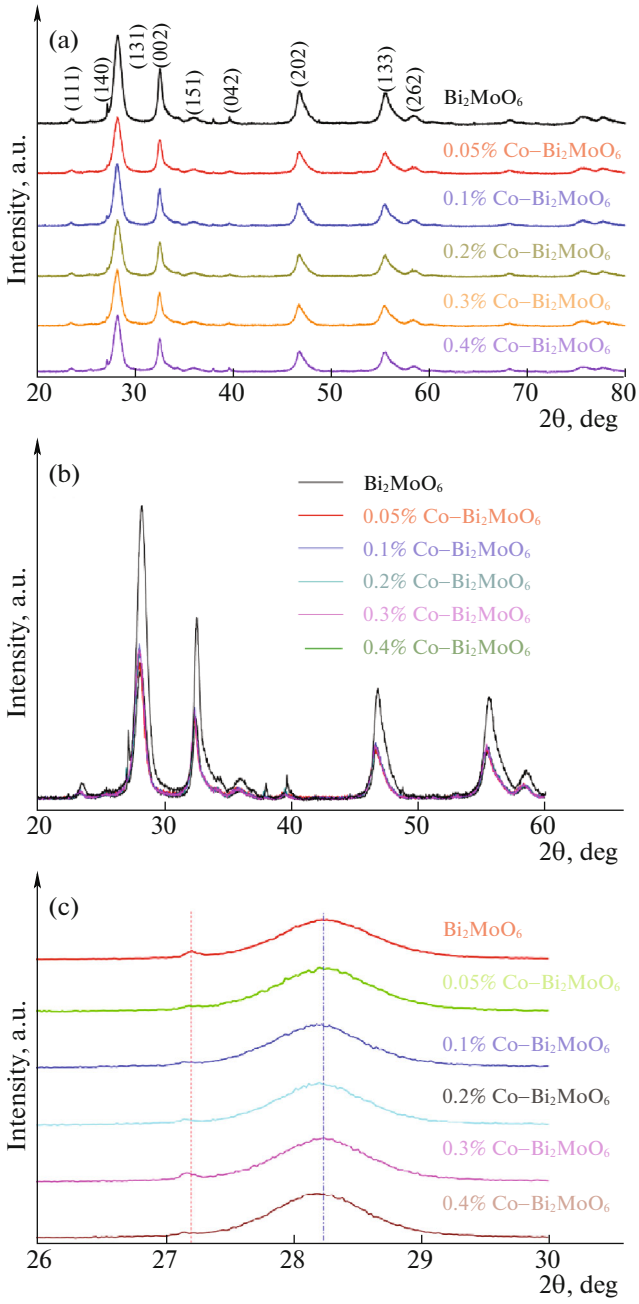

Fig. 1. (Color online) (a, b) XRD patterns of pure-Bi_2MoO_6 and Co-doped Bi_2MoO_6 samples, (c) magnified patterns of (140) and (131) crystal plane of pure-Bi_2MoO_6 and Co-doped Bi_2MoO_6 samples.

3.2. UV–Vis Spectra of the Products

The UV–Vis absorption spectra of pure-Bi_2MoO_6 and Co doped Bi_2MoO_6 composites are showed in Fig. 5. The absorption edge of pure-Bi_2MoO_6 is around 501 nm (E_g = 2.48 eV), indicating that Bi_2MoO_6 possesses strong photo absorption from the UV to visible-light region [28–30]. Co doping slightly affected the light absorption of Bi_2MoO_6 crystal and led to an obvious red-shift in the absorption threshold except 0.05% Co–Bi_2MoO_6 sample, indicating a decrease in the band gap. Moreover, 0.1% Co–Bi_2MoO_6 sample clearly shows the stronger absorption in the visible light range (450–800 nm) in comparison with pure-Bi_2MoO_6. It suggested that Co doping can obviously enhance the visible light harvesting ability of 0.1% Co–Bi_2MoO_6 sample, which could benefit an increase in visible light photocatalytic performance.

Fourier transform infrared (FTIR) spectra of pure-Bi_2MoO_6 and Co-doped Bi_2MoO_6 over the wave

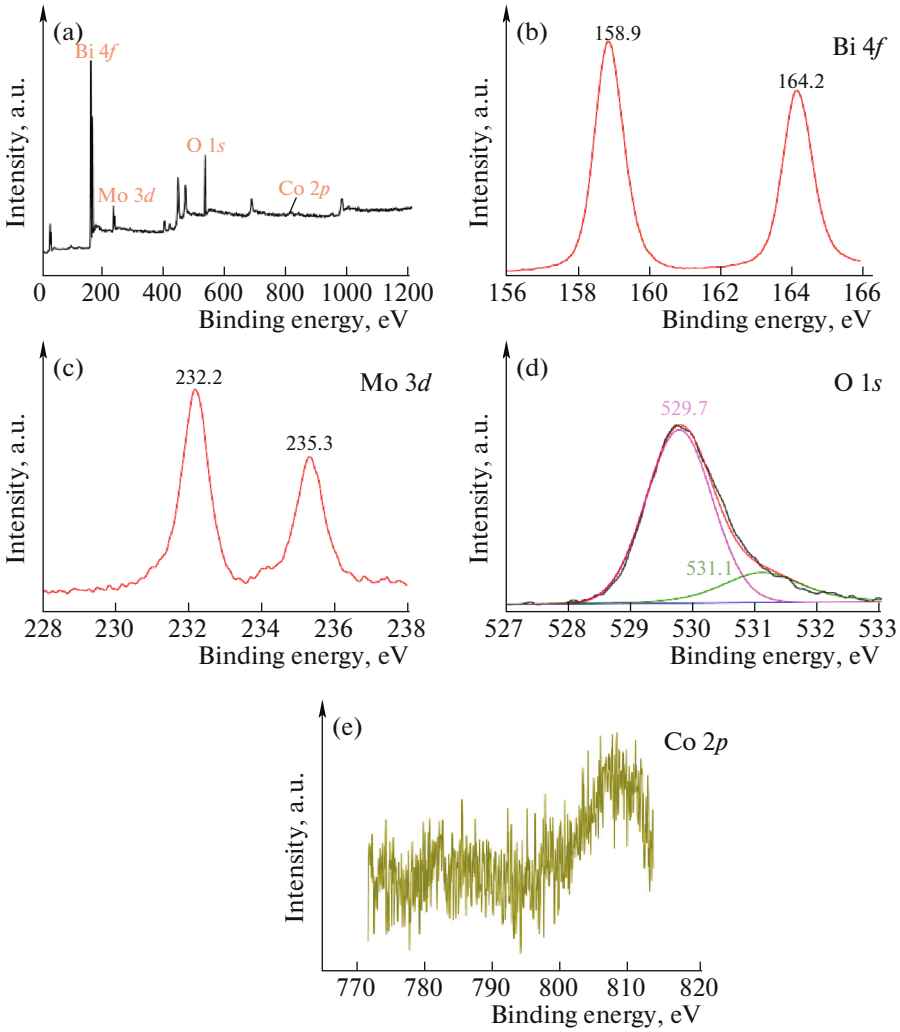

Fig. 2. (Color online) XPS spectra of 0.1% Co–Bi_2MoO_6 sample: (a) survey spectrum; (b) Bi4*f*, (c) Mo 3*d*, (d) O 1*s*, (e) Co 2*p*.

number of 600–2000 cm^{-1} are presented in Fig. 6. The FITR band at 717 cm^{-1} corresponds to the asymmetric stretching of Mo–O relating to vibration of the equatorial oxygen atoms in MoO_6 octahedrons. The absorption bands at 791 and 842 cm^{-1} are assigned to the asymmetric and symmetric stretching modes of Mo–O vibration of the apical oxygen atoms, respectively [20, 31]. The intensity of the bands at 717, 791, and 842 cm^{-1} appears slight decrease with the increase of Co concentration. The variations for the IR peaks further confirmed that Co could be successfully doped into the crystal lattice of Bi_2MoO_6.

3.3. Photocatalytic Activity of the Products

The photocatalytic performances of pure-Bi_2MoO_6 and Co-doped Bi_2MoO_6 samples were investigated by a degradation of Rhodamine B (RhB). Prior to the irradiation, the adsorption in the dark for 60 min was conducted so as to establish the adsorption/desorption equilibrium, and the absorbance value of aqueous RhB is 0.814. The corresponding photocatalytic properties have been demonstrated in Fig. 7. Figure 7a presents the temporal evolution of the absorption spectra of RhB solution over 20 mg of 0.1% Co–Bi_2MoO_6 as a catalyst after exposure to visible light. It could be seen that the characteristic absorption peak of RhB is located at 554 nm. After 60 min, the absorbance value of aqueous RhB reached 0.023, and after 80 min, the absorbance value of aqueous RhB achieved 0.006. The absorbance value of RhB solution decreases rapidly with extension of exposure time, and completely disappears after about 120 min, confirming that the RhB solution can be effectively photodegraded by the 0.1% Co–Bi_2MoO_6.

Figure 7b depicts the variation of RhB relative concentration C/C_0 with time over pure-Bi_2MoO_6, P25, 0.05% Co–Bi_2MoO_6, 0.1% Co–Bi_2MoO_6, 0.2% Co–Bi_2MoO_6, 0.3% Co–Bi_2MoO_6, 0.4% Co–Bi_2MoO_6, and blank RhB solution under the illumination of vis-

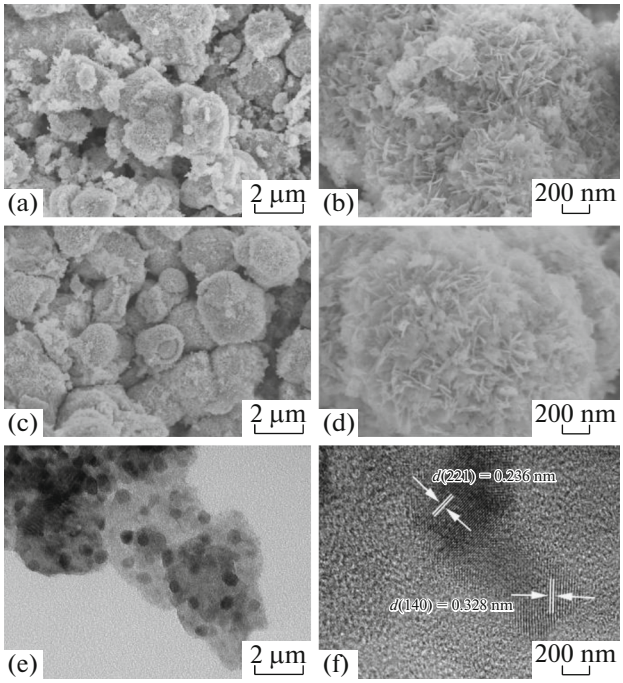

Fig. 3. SEM images of (a, b) pure-Bi_2MoO_6 and (c, d) 0.1% Co–Bi_2MoO_6, (e, f) TEM images of 0.1% Co–Bi_2MoO_6.

ible light. 6.9% of RhB solution is degraded without the photocatalyst after visible light irradiation for 120 min. The 0.1% Co–Bi_2MoO_6 show much higher photocatalytic performance than other samples, and the degradation percentage of RhB is up to 99.7% after 120 min. When pure-Bi_2MoO_6, P25, 0.05% Co–Bi_2MoO_6, 0.2% Co–Bi_2MoO_6, 0.3% Co–Bi_2MoO_6, and 0.4% Co–Bi_2MoO_6 were used as the photocatalyst, the degradation rate of RhB reached to 60.5, 66.9, 93.9, 90.2, 86.7, and 65.6%, respectively. Among them, 0.1% Co–Bi_2MoO_6 displays the highest activity, indicating the optimal molar ratio of Co/Bi is 0.001/1. In comparison with other Bi_2MoO_6 morphologies for degradation of RhB [32, 33], the present Co–Bi_2MoO_6 nanostructures exhibited excellent photocatalytic performance. Moreover, the mineralization ability of $Bi_2MoO_6$to RhB dye under visible-light irradiation were proved by different researchers [3, 29, 32], and confirming that Co–Bi_2MoO_6 can efficiently mineralize organic pollutant (RhB) under visible light.

The photocatalytic degradation kinetics of RhB was investigated in order to better understand the photocatalytic efficiency of our products. The degradation data were fit using a pseudo-first-order model, $\ln(C/C_0) = kt$, where k is the reaction rate constant, and t is the light irradiation time. The reaction rate constant k, which is equal to the corresponding slope of the fitting line, is shown in Fig. 7c. The k value of RhB over pure-Bi_2MoO_6, 0.05% Co–Bi_2MoO_6, 0.2% Co–Bi_2MoO_6, 0.3% Co–Bi_2MoO_6, and 0.4% Co–Bi_2MoO_6 are lower than that of 0.1% Co–Bi_2MoO_6. Notably, 0.1% Co–Bi_2MoO_6 (0.0298 ± 0.0028 min^{-1}) achieves the highest degradation rate among these samples, which is 4.18, 1.44, and 1.74 times higher than that of pure-Bi_2MoO_6 (0.0071 ± 0.0010 min^{-1}), 0.05% Co–Bi_2MoO_6 (0.0207 ± 0.0021 min^{-1}), and 0.2% Co–Bi_2MoO_6 (0.0171 ± 0.0016 min^{-1}), respectively. A five-cycle experiment was conducted for the photocatalytic degradation of RhB over the 0.1% Co–Bi_2MoO_6 to evaluate their stability, which is an important factor for the practical applications. Figure 7d illustrates the five cycles of variation in RhB relative concentration C/C_0 with irradiation time over 0.1% Co–Bi_2MoO_6 catalysts.

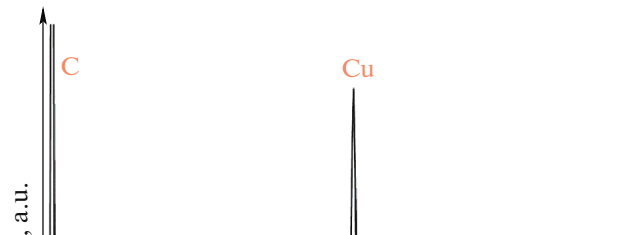

Fig. 4. (Color online) EDS pattern of 0.1% Co–Bi_2MoO_6.

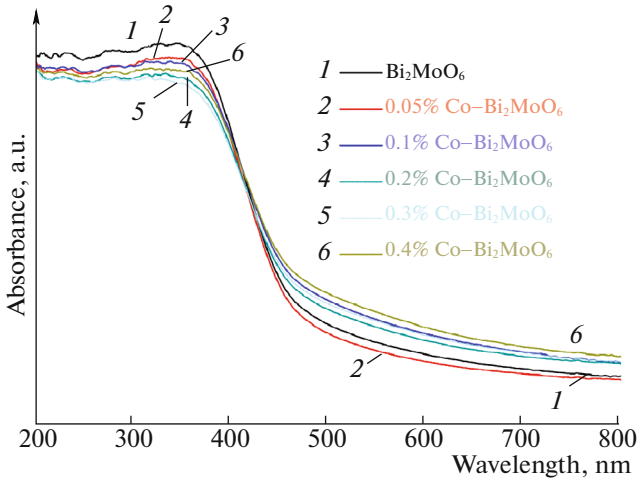

Fig. 5. (Color online) UV–Vis spectra of pure-Bi_2MoO_6 and Co-doped Bi_2MoO_6 samples.

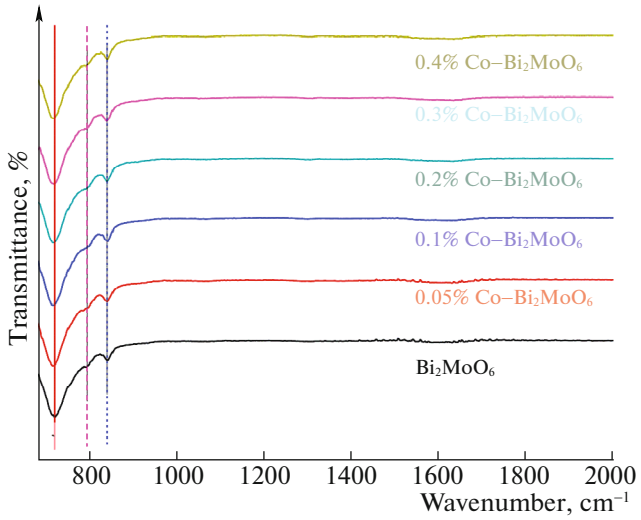

Fig. 6. (Color online) IR spectra of pure-Bi_2MoO_6 and Co-doped Bi_2MoO_6 samples.

The values of degradation rate are 98.0, 98.7, 95.4, 90.3, and 90.1%, for the first, second, third, fourth, and fifth runs, respectively. After five consecutive runs, there is only a slight loss of the photocatalytic activity, demonstrating the high photocatalytic stability of 0.1% Co–Bi_2MoO_6 catalysts. Comparing these samples, 0.1% Co–Bi_2MoO_6 has better degradation activity, which indicates Co doping played key roles in the enhanced photocatalytic performance. The enhancement may be due to the following reasons. Firstly, the higher photocatalysis efficiency of the 0.1% Co–Bi_2MoO_6 samples could be explained in terms of the enhancement of UV–Vis absorbance spectra due to Co doping. The enhancement of UV–Vis absorbance spectra of the 0.1% Co–Bi_2MoO_6 samples represents the optimized absorption property, offering the higher photocatalytic activity. Secondly, the results of XRD indicated that the average crystallite size of Bi_2MoO_6 was slightly decreased by Co doping. The decrease in crystal size lead to the increase of surface area for 0.1% Co–Bi_2MoO_6, and benefit the light harvesting and dye adsorption. Therefore, 0.1% Co–Bi_2MoO_6 exhibit higher catalytic activity than other samples.

4. CONCLUSIONS

The flower-like microspheres of pure-Bi_2MoO_6 and Co-doped Bi_2MoO_6 as visible-light-driven photocatalysts have been successfully synthesized through a sample and facile solvothermal method. The characterization results of XRD, XPS, SEM, and TEM show that all products were identified to the orthorhombic Bi_2MoO_6 microspheres composed of nanoplates. The

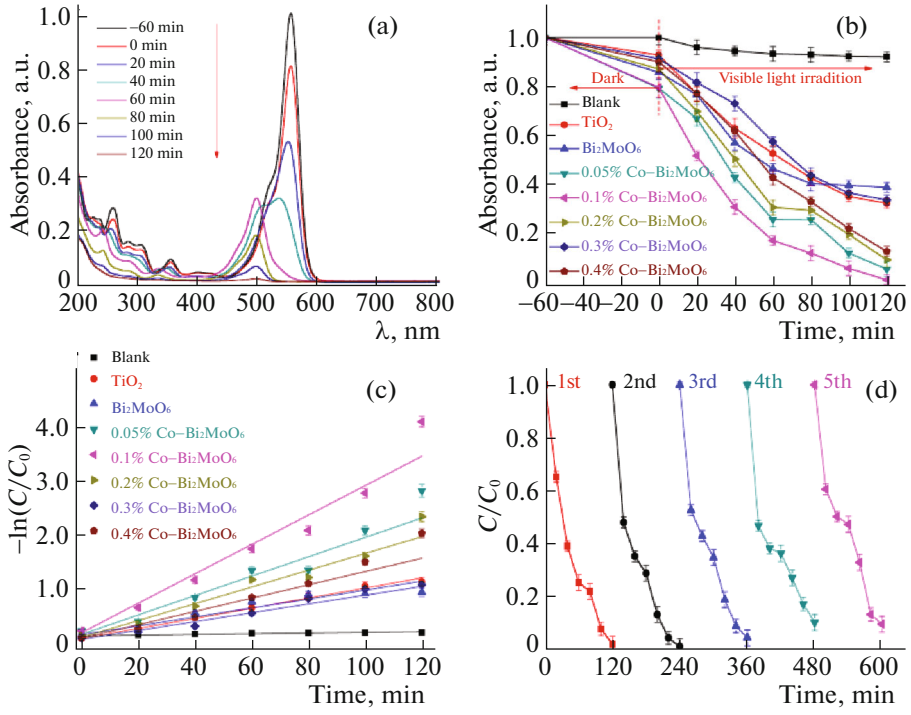

Fig. 7. (Color online) (a) The absorption spectra of RhB solution versus visible-light irradiation time in the presence of 0.1% Co–Bi_2MoO_6; (b) the degradation curves of RhB solution over different catalysts; (c) kinetic linear simulation curves of RhB photocatalytic degradation over different samples under visible light; (d) five cycles in the photocatalytic decomposition of RhB over 0.1% Co–Bi_2MoO_6.

photocatalytic degradation of RhB by pure-Bi_2MoO_6, P25, 0.05% Co–Bi_2MoO_6, 0.05% Co–Bi_2MoO_6, 0.1% Co–Bi_2MoO_6, 0.2% Co–Bi_2MoO_6, 0.3% Co–Bi_2MoO_6, and 0.4% Co–Bi_2MoO_6 as photocatalysts was investigated under visible-light irradiation. Among them, the 0.1% Co–Bi_2MoO_6 shows the highest photocatalytic performance for degradation of RhB within 120 min, and the degradation rate of 0.1% Co–Bi_2MoO_6 is 4.18, 1.44, and 1.74 times higher than that of pure-Bi_2MoO_6, 0.05% Co–Bi_2MoO_6, and 0.2% Co–Bi_2MoO_6, respectively. The facilely prepared 0.1% Co–Bi_2MoO_6 products are promising materials in fields such as photocatalytic and optoelectronic applications.

ACKNOWLEDGMENTS

This research was supported by the Foundation of Shanghai University of Engineering Science (grant no. 2012gp13, E1-0501-15-0105), Innovation Program of Shanghai Municipal Education Commission (grant no. 14ZZ160), Open Fund of State Key Laboratory for Modification of Chemical Fibers and Polymer Materials, Donghua University (grant no. LK1209).

REFERENCES

1. X. Lin, J. Yu, and M. Jaroniec, Chem. Soc. Rev. **45**, 2603 (2016).
2. H. P. Li, T. X. Hu, R. J. Zhang, J. Q. Liu, and W. G. Hou, Appl. Catal., B **188**, 313 (2016).
3. S. Y. Wang, X. L. Yang, X. H. Zhang, X. Ding, Z. X. Yang, K. Dai, and H. Chen, Appl. Surf. Sci. **391**, 194 (2017).
4. Q. Xiang, B. Cheng, and J. Yu, Angew. Chem., Int. Ed. **54**, 11350 (2015).
5. Y. Zhao, G. Chen, T. Bian, C. Zhou, G. I. N. Waterhouse, L. Wu, C. Tung, L. J. Smith, D. O'Hare, and T. Zhang, Adv. Mater. **27**, 7824 (2015).
6. Y. Ma, Y. Jia, L. Wang, M. Yang, Y. Bi, and Y. Qi, Chem. Eur. J **22**, 5844 (2016).
7. H. Wang, L. Zhang, Z. Chen, J. Hu, S. Li, Z. Wang, J. Liu, and X. Wang, Chem. Soc. Rev. **43**, 5234 (2014).
8. M. Wang, J. Ioccozia, L. Sun, C. Lin, and Z. Lin, Energy. Environ. Sci. **7**, 2182 (2014).
9. M. Zhang, J. Xu, R. Zong, and Y. Zhu, Appl. Catal., B **147**, 229 (2014).
10. M. P. Rao, V. P. Nandhini, J. J. Wu, A. Syed, F. Ameen, and S. Anandan, J. Solid State Chem. **258**, 647 (2018).
11. L. Wu, J. Bi, Z. Li, X. Wang, and X. Fu, Catal. Today **131**, 15 (2008).
12. S. Cao, J. Low, J. Yu, and M. Jaroniec, Adv. Mater. **27**, 2150 (2015).
13. H. Li, Y. Zhou, W. Tu, J. Ye, and Z. Zou, Adv. Func. Mater. **25**, 998 (2015).
14. Y. G. Sun, L. Y. Cai, X. J. Liu, Z. Cui, and P. H. Rao, J. Phys Chem. Solids. **111**, 75 (2017).
15. X. D. Zhu, Y. L. Zheng, Y. J. Feng, and K. N. Sun, J. Solid State Chem. **258**, 691 (2018).
16. J. L. Zhang, L. S. Zhang, N. Yu, K. B. Xu, S. J. Li, H. L. Wang, and J. S. Liu, RSC Adv. **5**, 75081 (2015).
17. Z. Zhao, Y. Zhou, F. Wang, K. Zhang, S. Yu, and K. Cao, ACS Appl. Mater. Inter. **7**, 730 (2015).
18. Z. Li, X. Chen, and Z. Xue, CrystEngComm. **15**, 498 (2013).
19. Y. Ma, Y. Jia, Z. Jiao, M. Yang, Y. Qi, and Y. Bi, Chem. Commun. **51**, 6655 (2015).
20. M. Imani, M. Farajnezhad, and A. Tadjarodi, Mater. Res. Bull. **87**, 92 (2017).
21. L. Shi, L. Liang, F. Wang, J. Ma, and J. Sun, Catal. Sci. Technol. **4**, 3235 (2014).
22. M. Y. Zhang, C. L. Shao, P. Zhang, C. Y. Su, X. Zhang, P. P. Liang, Y. Y. Sun, and Y. C. Liu, J. Hazard. Mater. **225**, 155 (2012).
23. A. Phuruangrat, P. Dumrongrojthanath, B. Kuntalue, S. Thongtem, and T. Thongtem, Mater. Lett. **196**, 256 (2017).
24. A. Phuruangrat, P. Dumrongrojthanath, S. Thongtem, and T. Thongtem, Mater. Lett. **194**, 114 (2017).
25. Z. Dai, F. Qin, H. P. Zhao, J. Ding, Y. L. Liu, and R. Chen, ACS Catal. **6**, 3180 (2016).
26. Z. C. Wu, X. Wang, J. S. Huang, and F. Gao, J. Mater. Chem. A **6**, 167 (2018).
27. B. J. Tan, K. J. Klabunde, and P. M. A. Sherwood, J. Am. Chem. Soc. **113**, 855 (1991).
28. Y. S. Xu and W. D. Zhang, Appl. Catal., B **140**, 306 (2013).
29. J. L. Zhang, L. S. Zhang, N. Yu, K. B. Xu, S. J. Li, H. L. Wang, and J. S. Liu, RSC Adv. **5**, 75081 (2015).
30. Y. J. Chen, G. H. Tian, Y. H. Shi, Y. T. Xiao, and H. G. Fu, Appl. Catal. B: Environ. **164**, 40 (2015).
31. J. Zhao, Z. Liu, and Q. Lu, Dyes Pigments **134**, 553 (2016).
32. S. J. Li, S. W. Hu, J. L. Zhang, W. Jiang, and J. S. Liu, J. Colloid Interf. Sci. **497**, 93 (2017).
33. C. L. Yu, Z. Wu, R. Y. Liu, H. B. He, W. H. Fan, and S. S. Xue, J. Phys Chem. Solids **93**, 7 (2017).